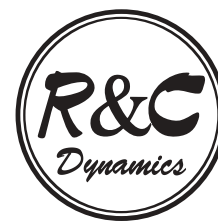


G. MAZE, X. CARTON, G. LAPEYRE

Laboratoire de Physique des Océans
IFREMER, BP70 - 29280 Plouzané
UBO 6, avenue Le Gorgeu
BP809 - 29285 Brest Cedex, France
E-mail: gmaze@univ-brest.fr
E-mail: Xavier.Carton@ifremer.fr
E-mail: glapeyre@ifremer.fr



DYNAMICS OF A 2D VORTEX DOUBLET UNDER EXTERNAL DEFORMATION

Received October 4, 2004

DOI: 10.1070/RD2004v009n04ABEH000291

The influence of an external strain (or shear) field on the evolution of two identical vortices is investigated in a two-dimensional incompressible fluid. Using point vortex modeling, two regimes of the vortex doublet (co-rotation and irreversible separation) are determined; the critical intensity of the large scale flow separating these two regimes for a given initial separation of vortices, is calculated. Finite-area effects are then considered for the vortices. The steady states of piecewise constant vortices are computed algebraically and numerically; positive strain (or shear) favors vortex deformation. This deformation has a dominant elliptical component. An elliptical model of two vortices confirms the point vortex model results for centroid trajectories, and the steady state model results concerning the influence of positive strain on vortex deformation. It also provides an estimate of critical merger distance in the presence of large scale flow. Finally, the finite-time, nonlinear evolution of the vortex doublet is simulated with a numerical code of the 2D vorticity equation. The various regimes (stationarity, merger, co-rotation, ejection) are classified in the plane of initial vortex separation and of external deformation. These regimes are analyzed, and the critical merger distance is evaluated for negative and positive external strain; the results are in agreement with the elliptical model prediction. Merger efficiency, defined as the ratio of final to initial vortex circulation, is computed; for the same initial distance, it is smaller for negative strain. It also depends in a more complex way of the initial vortex distance.

1. Introduction

Vortices are robust features of geophysical and experimental flows. The long life of geophysical vortices is now widely documented (see [5] for a review of observations and of mathematical theories of oceanic vortices). This robustness is due to strong internal dynamics, prevailing on large scale advection and deformation effects. But in-situ observations have also shown that oceanic vortices can exchange fluid when they are in close vicinity (see [19]). In the ocean, this interaction is rapid, and most often partial, insofar as only a small part of the vortex fluid is exchanged and as the two vortices still exist after the interaction, though with different sizes than initially.

In a different context (two-dimensional incompressible turbulence), vortex merger has been recognized as a key process for the growth of coherent vortices [16], [17]. Vortex merger is a fast, nonlinear process by which two vortices join and form a larger one which is initially elliptical [22]. Merger is defined as “complete” if its end product is a single vortex surrounded by filaments; it is partial if two distinct vortices eventually survive. In two-dimensional, free-decay turbulence, the inverse energy cascade is materialized by vortex merger, while the direct enstrophy cascade corresponds in physical space to the ejection of vorticity filaments during the merging process. Depending on viscosity and on the initial vortex structure, these filaments can be dissipated, allowing the final vortex to axisymmetrize, or the filaments can be wrapped around the vortex boundary and prevent its final axisymmetrization. In turbulent flows, merger catalysis by a third vortex has also been shown numerically.

Mathematics Subject Classification 76U05

These observations have prompted specific studies of vortex merger. For two identical Rankine¹ vortices, a critical distance has been found, beyond which vortices do not merge. This distance was assessed by several studies to lie in the range [3.16, 3.35] radii for two equal vortices [22], [8], [13], [20], [15]. But, both in turbulence and in nature, such symmetric initial conditions are rarely obtained and the two vortices differ in size or in intensity. The merger of two unequal vortices can be incomplete and lead to the formation of several end-products, among which vortices smaller than any of the former two [14]. A critical merger distance was calculated for two such vortices also [10], [23]. A weak efficiency of the merging process can also be due to other environmental factors, such as spatially-variable fluid thickness [2], anisotropic rate of global rotation (the so-called beta-effect of geophysical fluid dynamics) [1], barotropic instability of the vortices [4] or divergent flows which lead to cyclone-anticyclone asymmetry [7].

The merger of two vortices in a fluid free of large-scale currents is also an idealized situation: both in turbulence and in nature, vortices evolve in a large-scale deformation field (a shear or strain field due to non uniform currents or to neighboring vortices). The evolution of a single vortex in a large-scale deformation field is now well known: it becomes increasingly elliptical with imposed deformation, and limits to its robustness have been set, in terms of ratio of external deformation over internal vorticity [9].

The present paper is therefore concerned with the influence of such external deformation field on the evolution of two identical Rankine vortices (a preliminary investigation can be found in [6]). This problem is addressed here both with mathematical and numerical methods, and after recalling the framework of the study (section 2), the motion of the vortex centers is quantified via point vortex dynamics (section 3). The influence of finite vortex area on their merger are then investigated; steady states of the vortex doublet are computed and the idealization of the vortex as an ellipse provides a quasi-analytical description of its evolution (section 4). A numerical code of the nonlinear two-dimensional vorticity equation is then used to classify the various evolutions of finite-area vortex doublet and to calculate the physical characteristics of merger (critical merger distance, efficiency...; section 5). The influence of external deformation on merger efficiency and the localization of most deformed vortex regions are computed with an analytical criterion. Conclusions are finally drawn.

2. Mathematical and physical setting

Two dimensional incompressible, inviscid flows are governed by the vorticity equation:

$$\partial_t \zeta + J(\psi, \zeta) = 0 \quad (2.1)$$

where $\zeta = \nabla^2 \psi$ and ψ are the relative vorticity and streamfunction, and $J(a, b) = \partial_x a \partial_y b - \partial_x b \partial_y a$ is the Jacobian operator (x, y are Cartesian coordinates referenced to the center of the plane).

The initial conditions are two identical vortices (called “vortex doublet”), with unit vorticity and radius, located initially at $x = \pm d/2, y = 0$. The streamfunction is the sum of their contributions, of external strain and of solid-body rotation:

$$\psi = \psi_v - \frac{\Gamma}{2} (x^2 - y^2) + \frac{\Omega}{2} (x^2 + y^2)$$

The external flow field is a pure (linear) shear when $\Gamma = \pm \Omega$.

In section 5, Eq. 2.1 is implemented numerically to study the nonlinear evolution of the vortex doublet; the numerical scheme for this implementation is a pseudo-spectral decomposition in space (using fast Fourier transforms); horizontal resolution in physical space is 256^2 , with a square domain of length 2π . This numerical model performs time advection with a mixed Euler-leapfrog scheme. In this code, the null right-hand side of Eq. 2.1 is replaced by a hyper-viscosity operator $-(-1)^{n/2} \nu_n \nabla^n \zeta$; this

¹A Rankine vortex is a circular patch of constant relative vorticity in a 2D incompressible fluid

operator is a numerical procedure to eliminate the enstrophy accumulation at small scales, resulting from the turbulent cascade. This hyper viscosity does not alter the physical outcome provided n is large enough (here $n = 4$) and ν_n small enough (here $\nu_4 = 10^{-8}$). To avoid Gibbs instability with this numerical code, its initial conditions are slightly smoothed in vorticity (over two meshes) and the large scale deformation field is introduced only where vorticity exceeds a small threshold (5% of maximum vorticity).

3. Point vortex modeling

In the case of inviscid dynamics, we first assess the trajectory of the vortex centers by point vortex modeling.

3.1. Hamiltonian

Let us consider the case of two vortices with identical circulation κ . Their instantaneous positions are (ρ, θ) and $(\rho, \theta + \pi)$ in polar coordinates. Since the vorticity equation (2.1) conserves total energy because dissipation is neglected, vortex motion is determined by the Hamiltonian

$$H = -\frac{\kappa^2}{4\pi} [\ln(2\rho) - 2\gamma\rho^2 \cos(2\theta) + 2\omega\rho^2] \tag{3.1}$$

where we have set $\gamma = \pi\Gamma/\kappa$ and $\omega = \pi\Omega/\kappa$. We assume $\gamma > 0$ since a change of sign of γ is equivalent to a rotation of the axes. The radial and azimuthal velocities of each point vortex relatively to the center of the plane are

$$\begin{aligned} v_r = \dot{\rho} &= \frac{1}{\kappa\rho} \partial_\theta H = -\frac{\kappa}{\pi} \gamma\rho \sin(2\theta) \\ v_\theta = \rho\dot{\theta} &= -\frac{1}{\kappa} \partial_\rho H = \frac{\kappa}{2\pi} \left[\frac{1}{2\rho} - 2\gamma\rho \cos(2\theta) + 2\omega\rho \right] \end{aligned} \tag{3.2}$$

Figure 1 shows three plots of the Hamiltonian isolines in polar coordinate plane for three values of γ and ω . These three diagrams are themselves presented in the (ρ, θ) plane. For $\omega > \gamma$, the planar representation of the Hamiltonian shows that all trajectories are closed. Otherwise, there exists open or closed trajectories, separated by a fixed point in the polar coordinate plane.

Fixed points are given by $\dot{\rho} = \dot{\theta} = 0$, leading to

$$\theta_s = 0, \quad \rho_s = \frac{1}{2\sqrt{\gamma - \omega}}$$

for $\gamma - \omega > 0$. There also exists the solution

$$\theta_c = \pi/2, \quad \rho_c = \frac{1}{2\sqrt{-\gamma - \omega}}$$

when $\gamma + \omega < 0$. Recall that, owing to the symmetry, θ is defined in $]-\pi/2, \pi/2[$.

Stability of these fixed points is easily obtained from Eq.3.2. The eigenvalues of the Jacobian matrix

$$J = \begin{pmatrix} \frac{\partial \dot{\rho}}{\partial \rho} & \frac{1}{\rho} \frac{\partial \dot{\rho}}{\partial \theta} \\ \frac{\partial \dot{\theta}}{\partial \rho} & \frac{1}{\rho} \frac{\partial \dot{\theta}}{\partial \theta} \end{pmatrix}$$

are, for $\theta = 0$,

$$\lambda_{s,\pm} = \pm \frac{2\kappa}{\pi} \sqrt{\gamma(\gamma - \omega)}.$$

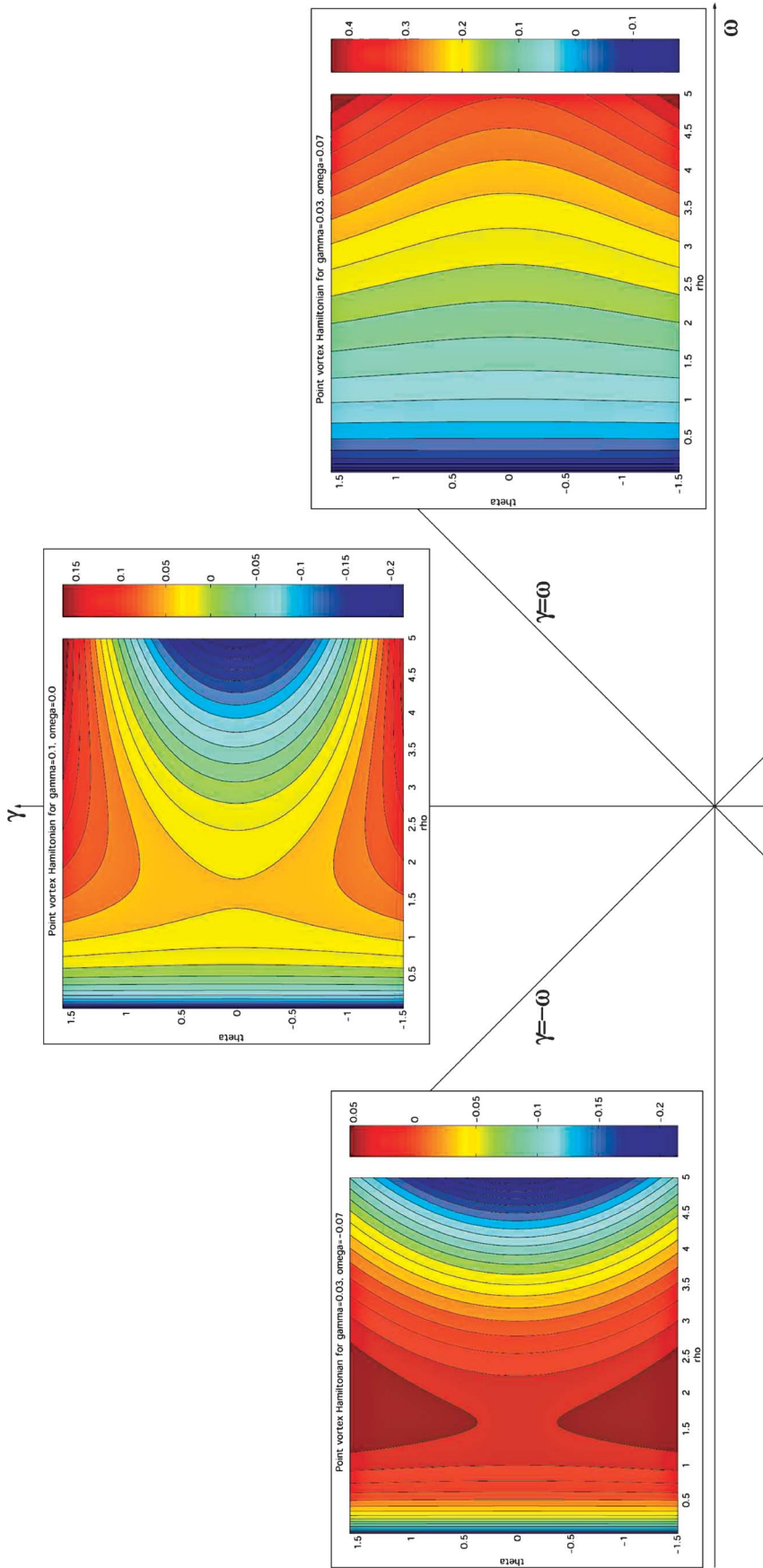


Fig. 1. Three plots of Hamiltonian isolines (each of them in the polar coordinate plane) for a vortex doublet (with $\kappa = \pi$), in the (ω, γ) parameter plane. The three plots of $H(\rho, \theta)$ correspond respectively to $\omega = 0.07, \gamma = 0.03, \omega = 0, \gamma = 0.1, \omega = -0.07, \gamma = 0.03$

They are of opposite sign so that this fixed point is a saddle point. It is easily shown (either by computing the associated eigenvectors or by calculating the second order derivatives of H in ρ and θ) that this fixed point is stable/unstable with respect to radial/angular disturbances.

For $\theta = \pi/2$, the eigenvalues are

$$\lambda_{c,\pm} = \pm i \frac{2\kappa}{\pi} \sqrt{\gamma(-\gamma - \omega)}$$

so that this fixed point is a center.

This analysis is illustrated by figure 1: for $0 < \gamma < \omega$, no fixed point is observed. For $\gamma > |\omega|$, only the saddle point is present; it separates open and closed trajectories. Conversely, for a given initial separation $2\rho_f$ between the vortices, $\gamma - \omega$ will be the critical value of external deformation separating open and closed trajectories. For $0 < \gamma < -\omega$, both the saddle point and the centers exist in the (ρ, θ) plane.

3.2. Trajectories

For zero deformation field, the vortex trajectories are circles:

$$\rho = \rho_0, \quad \theta = \theta_0(t) = \frac{\kappa t}{4\pi\rho^2}.$$

Assuming a weak deformation flow and setting $0 < \gamma \ll 1$, $0 < \omega \ll 1$, the vortex trajectories can be obtained in perturbation expansion in γ and ω :

$$\begin{aligned} \rho &= \rho_0 + \gamma f(t) = \rho_0 + 2\gamma\rho_0^3 \cos(2\theta_0(t)), \\ \theta &= \theta_0(t) + \gamma g(t) = \theta_0(t) - 3\gamma\rho_0^3 \sin(2\theta_0(t)) + \omega \frac{\kappa\rho_0 t}{\pi}. \end{aligned}$$

The assumption of a weak deformation imposes small distances from the center of the plane. Therefore, internal trajectories (i.e. trajectories bounded by the fixed point) are ellipses at first order in γ (see again figure 1). Their aspect ratio and ellipticity are

$$\lambda = \frac{1 - 2\gamma\rho_0^2}{1 + 2\gamma\rho_0^2}, \quad e = 4\gamma\rho_0^2.$$

This result can also be obtained directly from the Hamiltonian by setting $\rho = \rho_0/(1 + e \cos(2\theta))$ and by cancelling the 2θ part, leading to $e = 4\gamma\rho_0^2$.

4. Steady states of piecewise-constant vortices

After assessing the vortex trajectories, we determine their deformation under stationary conditions, both analytically and numerically.

4.1. Approximate analytical solution

Under the hypothesis of stationarity, each vortex boundary is computed by perturbation expansion, assuming that the vortex deformation is weak. In steady configuration, the vortex boundary is a streamline of the total flow (induced by the companion vortex and the large-scale deformation field). The companion vortex is idealized here as a point vortex located at its center and having its total circulation. The mathematical technique used to compute the stationary contour deformation is extensively explained in [8] and is not recalled in detail here.

The vortex radius is $r = 1 + \eta(\alpha)$ where η is the contour deformation from a circle, and α is the local angle (relative to the vortex center; see figure 2). The contour deformation η is expanded in

powers of $\epsilon = 1/d$ and the order ϵ^n term is assumed of the form $\cos(n\alpha) - 1$. Let γ and ω be at most of order $O(\epsilon^2)$. Stationarity is given by

$$\frac{\partial\psi}{\partial r} \frac{d\eta}{d\alpha} = -\frac{\partial\psi}{\partial\alpha}. \tag{4.1}$$

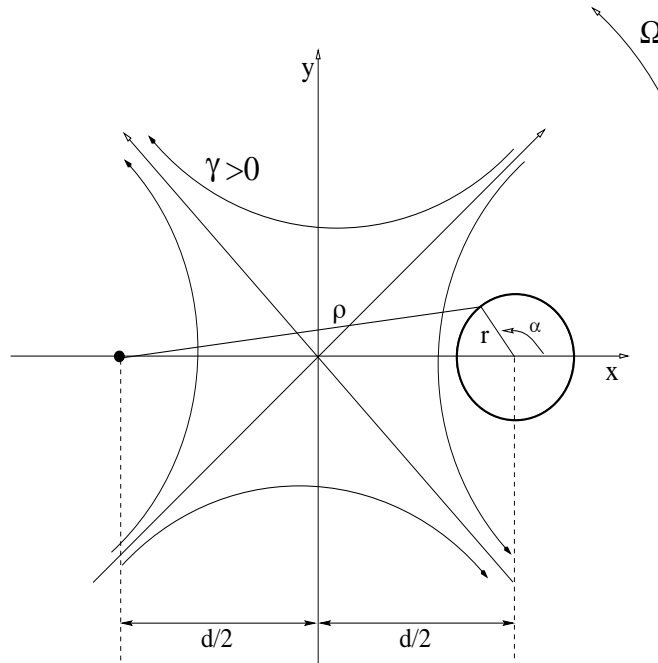


Fig. 2. Idealized flow configuration for the calculation of steady states: a piecewise-constant vortex is influenced by the large-scale field and by a distant point vortex

At order ϵ , the condition for stationarity of the vortex center (already obtained with point vortices) is recovered

$$1 - (\gamma - \omega) d^2 = 0 \tag{4.2}$$

assuming $\gamma > 0, \gamma > \omega$.

At order ϵ^2 , the elliptical deformation of the vortex contour is

$$\eta_2 = \eta_0[\cos(2\alpha) - 1], \quad \eta_0 = \frac{1 + 2\gamma d^2}{1 + 2\omega}. \tag{4.3}$$

We note that under zero external deformation the classical result $\eta_0 = 1$ is recovered [8].

4.2. Numerical solution

The steady states of the vortex doublet are now computed numerically; the algorithm is based on the same principle as above: the steady vortex contour is a streamline of a total field and it has zero total rotation rate. This steady vortex contour is computed iteratively with two Newton-Raphson procedures.

Starting from a first guess of circular vortices with rotation rate given by point vortex theory, the vortex boundaries on the x-axis are fixed as abscissae $\rho_f - 1$ and $\rho_f + 1$, with $\rho_f = 1/(2\sqrt{\gamma - \omega})$. The $N - 2$ other ordinates of the vortex contour, the rotation rate and the (constant) value of the streamfunction on the contour represent the other unknowns. The derivative of the total streamfunction with respect to these variables is used in a Newton-Raphson procedure to obtain a first steady state (with non zero rotation rate). A second steady state is obtained with center $\rho_f - 0.05$ with

a different rotation rate. With these two seeds, a second Newton-Raphson procedure, based on the displacement of the vortex center, converges towards zero rotation rate. The final position of the vortex center ρ_{num} is then obtained. The area of the steady vortex is A_{num} (remember that, assuming ellipticity the theoretical value is $A_{th} = \pi(1 - 2\epsilon^2\eta_0)$ using the formula hereabove).

4.3. Analysis of numerical solutions and comparison with analytical solutions

First, the theoretical and the numerical positions of steady vortex centers are compared for various values of γ and ω (see figure 3). In the absence of external deformation, the relative difference between theory and numerics is at most 1% (the numerical value being slightly larger than the theoretical one). When external deformation is applied, discrepancies can rise to 23% for maximum values of γ and ω allowing the existence of steady states.

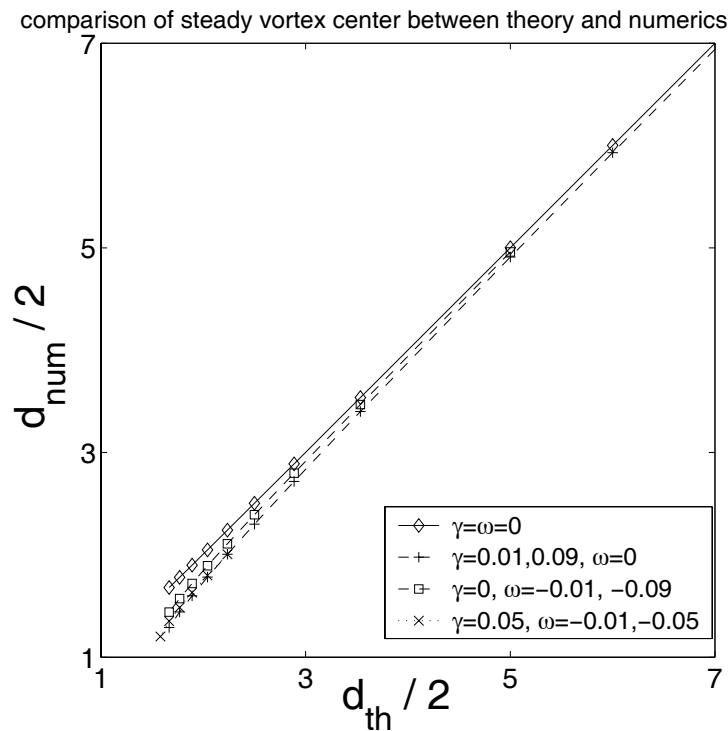


Fig. 3. Comparison of stationary vortex center position between theory and numerical experiments ($d_{th}/2 = \rho_f$), for various values of γ and ω

Secondly, the theoretical and the numerical areas of steady vortices are compared for the same values of γ and ω (see figure 4). In the absence of external deformation, the relative difference between theory and numerics is at most 2% (the numerical value being slightly smaller than the theoretical one). When external deformation is applied, differences can also rise to 23% for limiting states (discrepancies being larger for pure strain than in presence of external rotation).

Finally, the steady vortex contours are Fourier analyzed in α and the amplitude of each mode ($m = 1 - 4$) is plotted versus $\rho_f = d_{th}/2$ (see figure 5a), in the case of pure strain (other cases are similar). This analysis shows that the elliptical mode ($m = 2$) dominates the other angular modes by far. In this case, the square mode ($m = 4$) is five times less intense, and is followed in amplitude by the asymmetric mode ($m = 1$) and by the triangular one ($m = 3$). This can be related to the two-fold symmetry of the large-scale strain field. Indeed, in the absence of deformation, modes $m = 1, 3, 4$ have similar amplitudes. In the case of pure rotation, mode $m = 1$ is naturally favored.

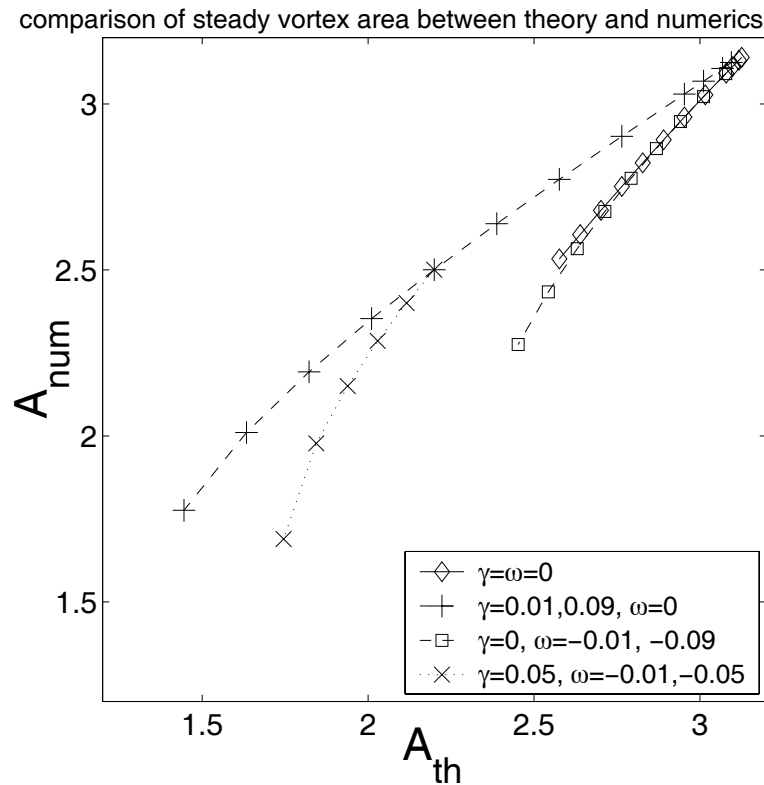


Fig. 4. Comparison of stationary vortex area between theory and numerical experiments (see text for definition of A_{th}), for various values of γ and ω

The amplitude of the elliptical mode is now compared between the various cases (no deformation, pure strain, pure rotation, mixed deformation). Figure 5b shows a 40% increase in elliptical mode amplitude when rotation is added. This increase is even more drastic (110%) in the presence of strain. Mixed deformation (strain+rotation) does not substantially change this increase from the pure strain case, but favors the growth of the asymmetric mode.

4.4. The elliptical model

The previous section has shown that the elliptical mode prevails in the deformation of the vortex contours at equilibrium. An elliptical vortex model, which retains only four degrees of freedom for each vortex (centroid position, aspect ratio, angle), should therefore be appropriate to describe the dynamics of the system as long as merger has not occurred. We apply this model to our problem following the algebra given by [13].

Calling $Z = x_c + iy_c$ the complex coordinate of the vortex centroid, $\lambda = b/a$ the aspect ratio of each vortex, and $e = [a^2 - b^2]/2 \exp(2i\phi)$ its ellipticity, with ϕ the angle between the major axis and the x -axis, the dynamical equations of the elliptical vortex are

$$\frac{dZ}{d\tau} = -i(\gamma Z^* - \omega Z) - [ZBC]^* \quad (4.4)$$

and

$$\frac{de}{d\tau} = i\left[e\left(\frac{1}{ab + F} + 2\omega\right) - F(2\gamma + i[C(B + e)]^*)\right] \quad (4.5)$$

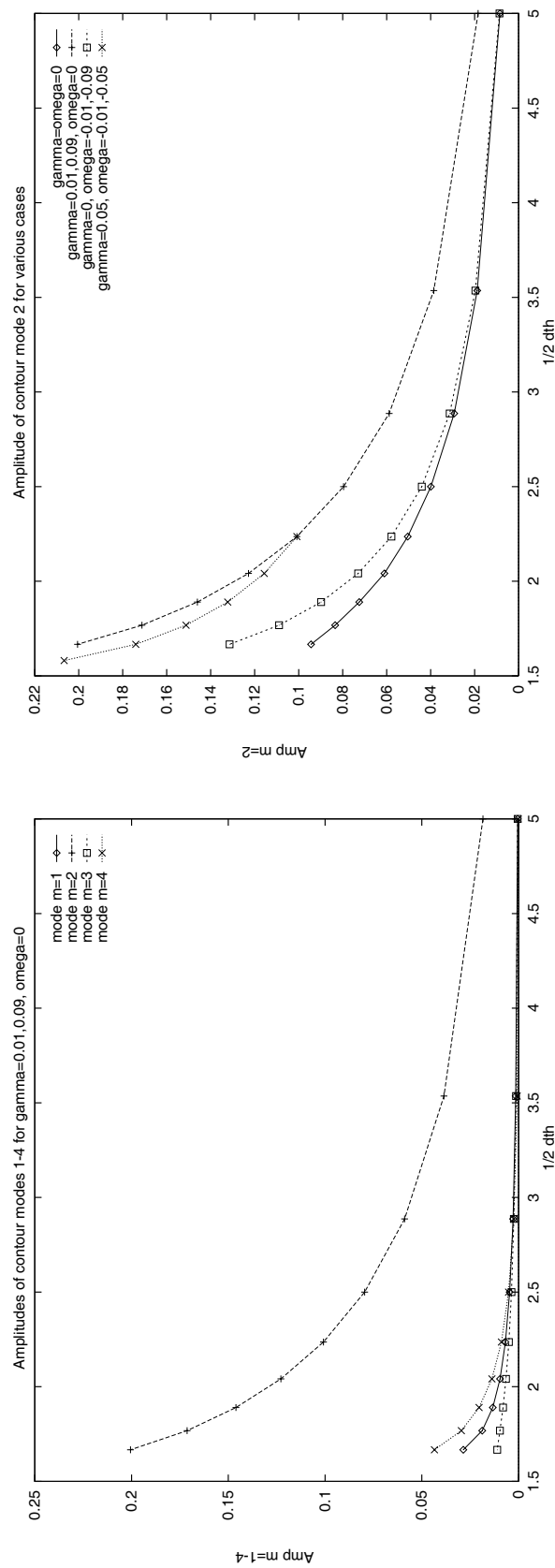


Fig. 5. (a) Amplitude of contour modes $m = 1 - 4$ versus theoretical distance of vortex center for pure strain case; (b) amplitude of elliptical mode $m = 2$ versus $d_{th}/2$ for various values of γ and ω

where the time scale has been normalized as $\tau = 4\pi\kappa t$, with the following parameters

$$B = 4Z^2 - e; \quad C = \frac{i}{B^2 - e^2}$$

$$F = \sqrt{a^2b^2 + |e|^2} = \frac{a^2 + b^2}{2}$$

Firstly, we use the elliptical model to confirm our analytical calculation of steady states; assuming that the vortices are weakly elliptical (with average radius unity and centroids located at $\pm d/2, 0$), the equations become:

$$B = d^2, \quad C = \frac{i}{d^2}, \quad F = 1$$

The equation for the motion of centroids is in stationary form:

$$(\gamma - \omega) d^2 - 1 = 0$$

which is the condition of no motion for point vortices, and the ellipticity equation is, again in stationary form:

$$e \left(\frac{1}{2} + \omega \right) - \left(\gamma + \frac{1}{d^2} \right) = 0$$

and using $e = 2\eta_0/d^2$, we obtain

$$\eta_0 = \frac{1 + 2\gamma d^2}{1 + 2\omega}$$

the value of contour deformation calculated in section 4.1.

Secondly, the elliptical model allows the computation of a critical distance between vortex centers under which merger should occur. At this distance, elliptical vortices exhibit a change in direction of rotation of their main axis [13]. The results are shown in table 1. Adding positive external strain reduces the domain of existence of steady states (thus favoring merger), but only up to a given strain amplitude. Beyond this value, merger is not favored any more; we will observe this behavior again in the nonlinear results of the spectral code (see section 5).

5. Nonlinear evolutions of the vortices

5.1. Nonlinear regimes: classification and analysis

The nonlinear pseudospectral code is now run with the initial conditions of two piecewise constant vortices in the large-scale deformation field. Two parameters are varied: the intensity of the strain (scaled by the unit vorticity of each vortex) and the initial intercentroid distance (scaled by the radius of each vortex here chosen as $r_0 = 0.3$ to avoid spurious periodicity effects).

Previous studies of vortex merger are used to determine the appropriate values of these parameters. In the absence of strain, two piecewise constant vortices merge if their intercentroid distance is smaller than a critical value; several estimates of this critical value, ranging between 3.16 and 3.35 radii, can be found in the literature [22], [8], [15], [13], [20]. Point vortex theory shows that vortices at this distance are stationary if $\gamma \sim 0.1$. Therefore, our choice for ranges of initial intercentroid distances will span [2, 5], and γ will most often vary between -0.2 and 0.2 (and exceptionally rise up to 0.8).

The time-series of vorticity plots obtained after each simulation allow the identification of four different regimes in the $[\gamma, d/r_0]$ plane:

— stationarity: if the initial distance between the vortex centers d is equal to $2\rho_f$, the two vortices become slightly deformed but do not move away from their initial position (see figure 6). In practice, this regime is difficult to obtain numerically since the two vortices have finite extent here, and since the fixed point position is unstable to azimuthal disturbances. High-resolution simulations (512x512) were necessary to locate this regime precisely in the parameter plane.

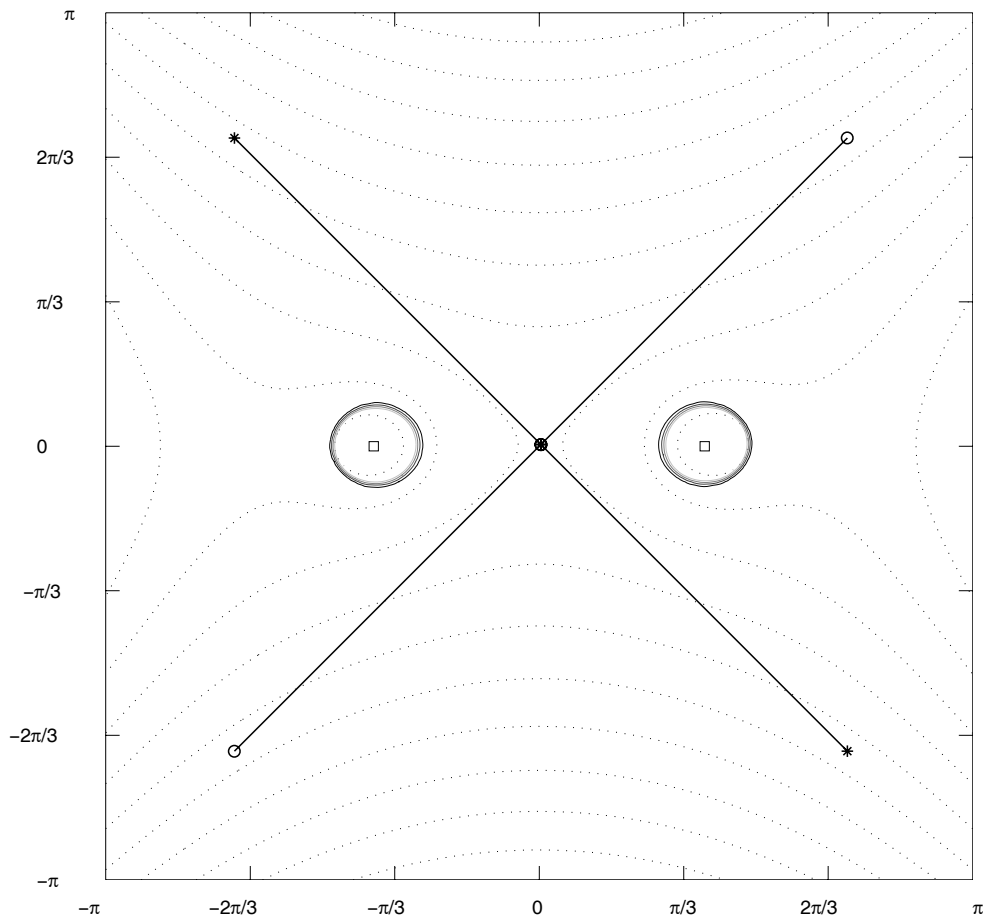


Fig. 6. Vortex stationarity. The Rankine vortices are bounded by the thick solid lines. Their initial positions are given by the small squares. Dashed lines denote the instantaneous streamlines. The two strain axes are indicated (circles on axis of compression and stars on axis of expansion)

— strain-induced expulsion: if the initial distance d between the vortex centers is larger than $2\rho_f$, the strain field is dominant in the vortex motion. The two vortices then drift apart, following open trajectories slightly different from the initial Hamiltonian isolines due to finite-size effects and to motion of the vortices in the fixed external flow (see figure 7).

— co-rotation: if the initial distance d between the vortex centers is smaller than $2\rho_f$ but larger than the critical distance for merger, the two vortices follow close, elliptical trajectories (see figure 8) as predicted by point vortex theory. When varying the intensity of the strain, the aspect ratio of these trajectories is nearly that given by the point vortex and elliptical models (see table 2). As expected, the stronger the strain, the more elongated the trajectory is. Each vortex shape is also close to elliptical with an aspect ratio predicted by the analytical solution (see table 3). Indeed, the relative difference in vortex ellipticity between the elliptical and spectral models is at most 9%.

— merger: since vortex merger is a fast nonlinear process, the long term effect of viscous dissipation can be neglected and the efficiency of vortex merger can be defined as the ratio of the circulation of the final vortex to the total circulation of the two initial vortices. To neglect viscous effects, we impose that merging process takes place within a rotation period of the vortex doublet.

Figure 9 shows the time series of vorticity plots for merger in a weak strain. The strain elongates the two vortices meridionally and slows down global rotation, at least initially; this latter point was already predicted by point vortex theory. Nevertheless, the global process of vortex merger with weak

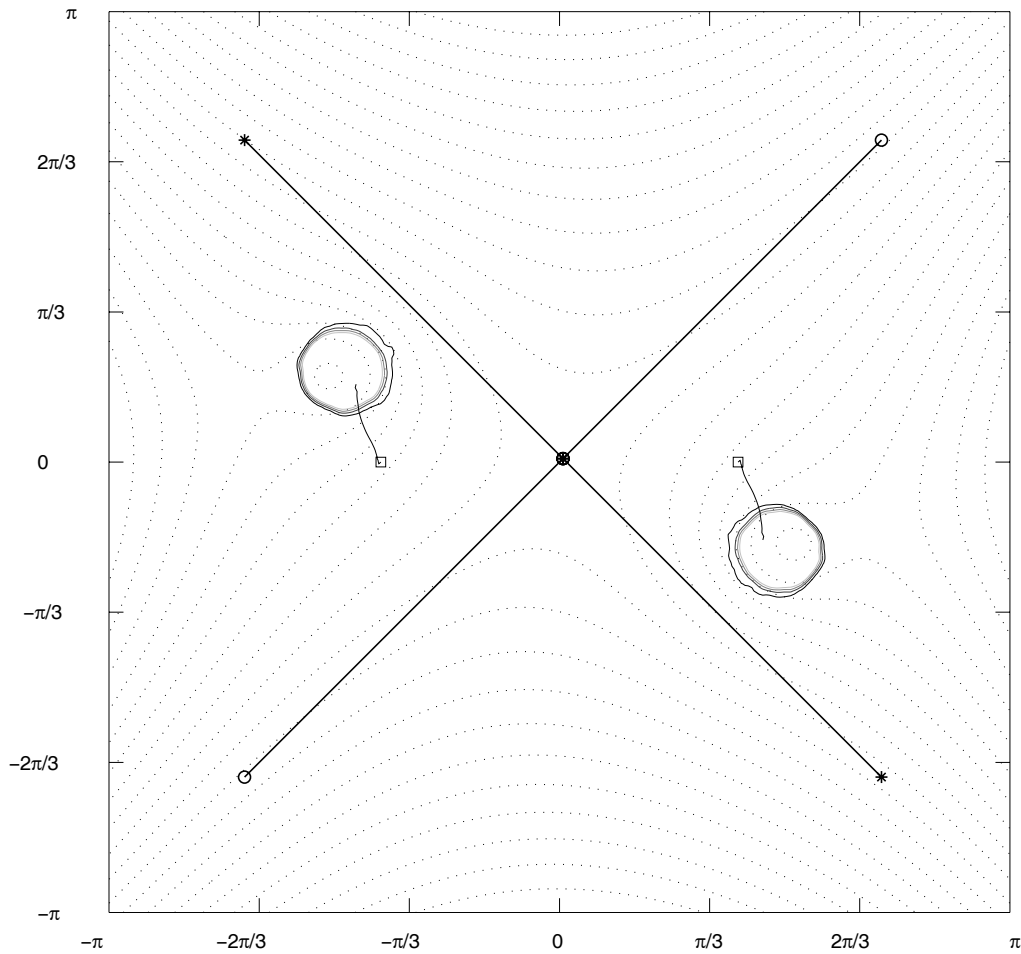


Fig. 7. Strain-induced ejection of vortices. The Rankine vortices are bounded by the thick solid lines. Their initial positions are given by the small squares and their trajectory by the thin solid line. Dashed lines denote the instantaneous streamlines. The two strain axes are indicated (circles on axis of compression and stars on axis of expansion)

large-scale strain is quite comparable to that without strain. Fluid is exchanged between the two structures near the center of the plane. Their collapse increases and the two vortex cores spiral down towards the center: their thinning cross-section allows fluid mixing and the formation of a single vortex at the center. Here, the strain rate is not sufficient to break this structure apart. Indeed, we recall that [9] has shown that a strain rate on order of 15% of the vorticity is required for an elliptical vortex to split apart.

Figure 10 presents the distribution of regimes in the $(\gamma, d/r_0)$ plane. Only two regimes (merger and co-rotation) exist in the absence of strain. Two other regimes are specific of strain effects: strain-induced expulsion and equilibria. In the presence of weak strain, vortices need to be initially very distant to be advected outwards. The curve separating the regimes of co-rotation and of strain-induced expulsion has $d/r_0 \sim 1/\sqrt{\gamma}$. This relation was already obtained by point vortex theory as a separation between open and close trajectories.

For weak positive strain, merger is favored. Still, this favorable influence of strain on critical merger distance reaches a maximum for $\gamma \sim 0.4$. Then, strain-induced vortex expulsion becomes the dominant process. This optimum value of strain can be considered as the limit of a background effect.

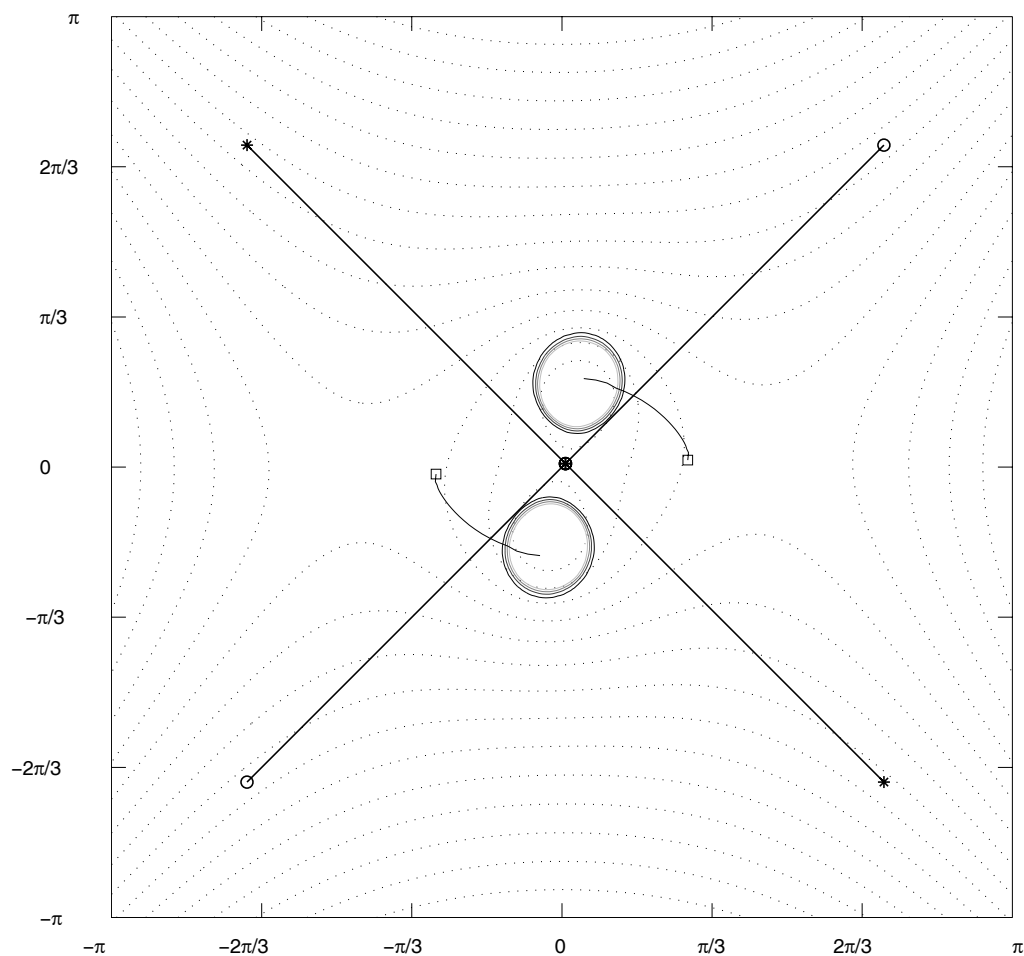


Fig. 8. Vortex co-rotation. The Rankine vortices are bounded by the thick solid lines. Their initial positions are given by the small squares and their trajectory by the thin solid line. The two strain axes are indicated (circles on axis of compression and stars on axis of expansion)

Indeed, strong strains have disruptive effects on coherent structures, among which that of breaking vortices.

5.2. Critical merger distance

Merger occurs only when vortices are initially close enough. This critical distance is influenced by strain as previous sections have indicated. The variation of this critical distance with strain is summarized in tables 4 and 5. With the specific orientation of the strain chosen here, a positive strain favors merger while a negative strain acts against it. Again, this is in agreement with the deformation of the vortices induced by their companion and by the large scale strain, computed with the steady state and elliptical models. Values of critical merger distance obtained with the spectral code show good correspondence with minimum distances for the existence of elliptical vortex doublets (3 % relative error).

The weaker influence of a negative strain than that of a positive strain on vortex merger can be explained by the variation of angular velocity with γ (see section 3.2). As recalled above, the doublet rotates more slowly in the first quadrant under positive strain and thus it can fully undergo the favorable influence of this strain on merger (in particular, via an increased deformation). On

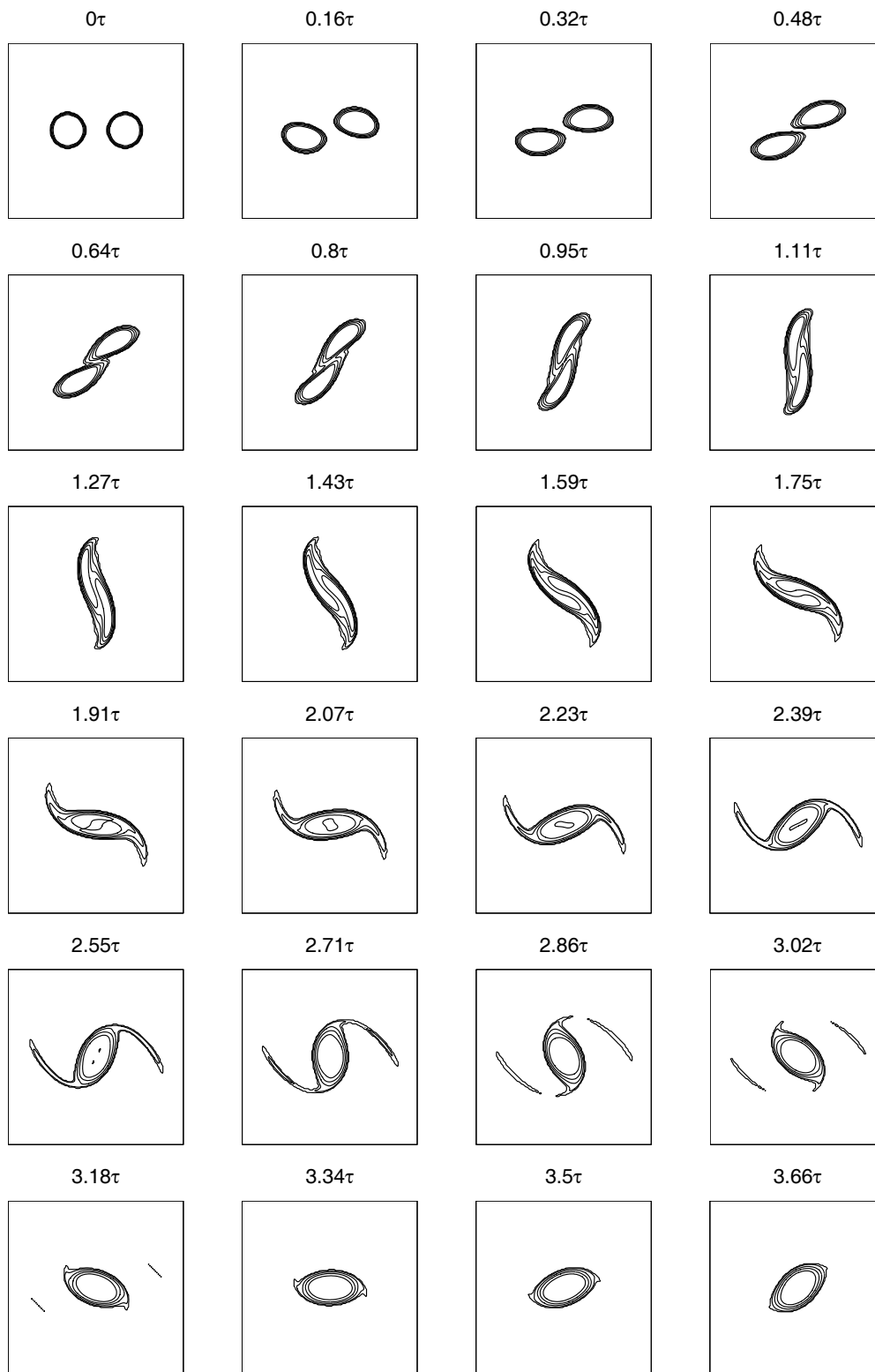


Fig. 9. Vortex merger. Time series of vorticity plots for merger of two vortices with uniform vorticity $\zeta = 1$, initially separated by a distance $d = 3.4 r_0$ in a weak strain ($\gamma = 0.18$). Evolution is from left to right and from top to bottom

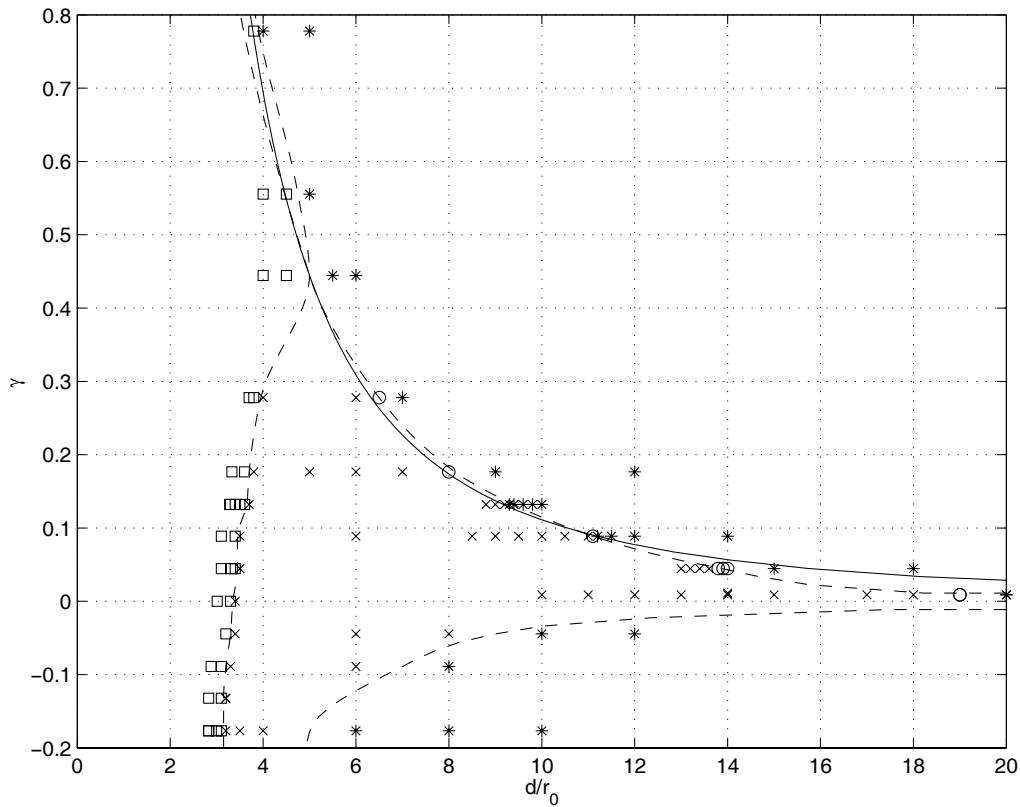


Fig. 10. Distribution of regimes in the $(\gamma, d/r_0)$ plane. Square: merger; cross: co-rotation; circle: stationarity; star: strain-induced expulsion. Dashed lines separate different regimes and solid line is point vortex stationarity (remember that $r_0 = 0.3$ in the spectral code)

the contrary, the vortex doublet rotates more rapidly in the first quadrant with negative strain, and therefore the negative effects of this strain on merger are felt for a shorter duration.

Finally, the influence of a non-zero rotation rate (ω) is assessed. Point vortex and steady state calculations have indicated that positive rotation has an effect opposite to that of positive strain on vortex doublet evolution: it favors elliptical trajectories and decreases each vortex ellipticity. Table 6 shows the variation of the critical merger distance for $\omega = \pm\gamma$, obtained with the spectral code and the elliptical model. The two models indicate the same tendency, namely the increase of critical merger distance with increasing external rotation. This positive influence of ω on co-rotation against merger is in agreement with the point-vortex and steady state results.

5.3. Filamentation analysis

The role of vortex deformation during merger and the resulting formation of filaments are evaluated here with the Lagrangian criterion on vortex filamentation, derived by [11]. This deformation is due to the combined action of the external strain γ and of the strain induced by the companion vortex. This criterion is based on a Lagrangian approach of tracer gradients; it predicts the exponential growth rate of tracer gradients and therefore the stretching and straining undergone by vortices. We recall that this rate is

$$\sigma^{eff} = \sqrt{\sigma^2 - (\zeta + 2\dot{\phi})^2}$$

(or zero if imaginary) where σ is the rate of deformation, ζ is vorticity and $\dot{\phi}$ is the rotation rate of the principal axes of deformation.

Firstly, we investigate the case with weak external deformation, using the criterion derived by [11] (see figure 11). Initially, the deformation is oriented along the doublet axis. It is more intense between the vortices and less intense on the outer side ². This induces an asymmetry in vortex deformation by stretching the inner side more than the outer side of the vortices (as seen at $t = 0.64\tau$). The vortex centroids will then collapse towards the center of the plane with maximum deformation still aligned along the doublet axis, and concentrated near the cusps of their contours. This concentration will induce vortex splitting, accompanied by the ejection of peripheral filaments (cf. $t = 1.11\tau$ and $t = 1.43\tau$). During merger, the low-vorticity region between vortex cores is strongly deformed and elongated; it will rapidly disappear (at $t = 2.55\tau$). Merger thus seems favored by this stronger deformation on the inner side of the vortices: more fluid will be advected inwards than outwards leading to the collapse of centroids.

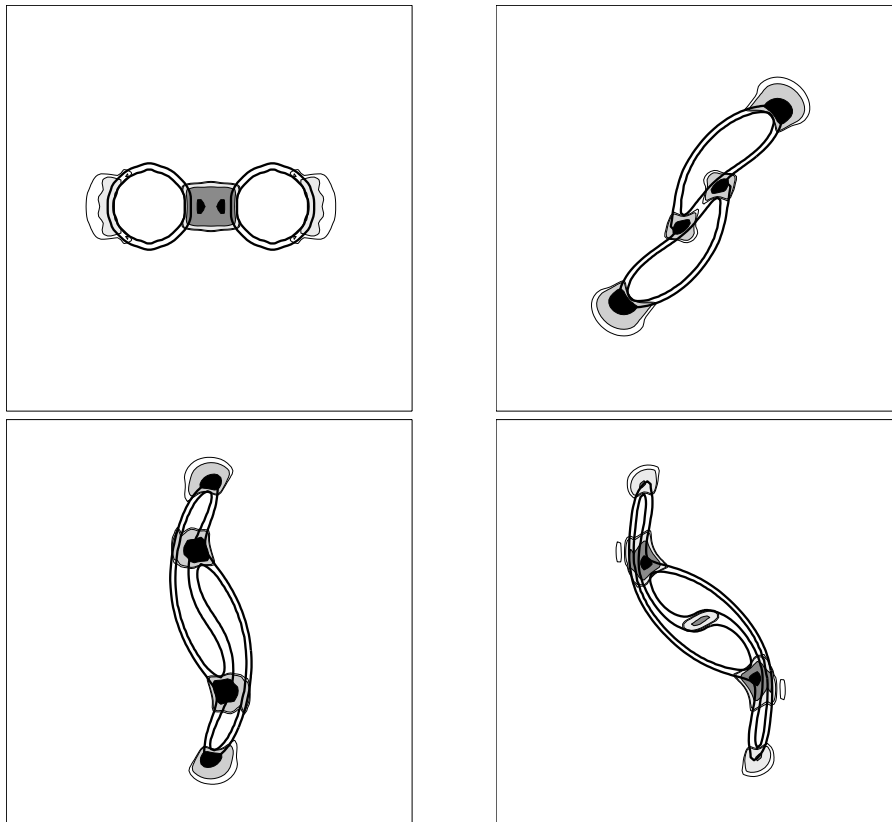


Fig. 11. Effective rate of deformation by Lapeyre et al (1999) criterion at time $t = 0, 0.64\tau, 1.11\tau, 1.43\tau$ for the simulation of figure 9. In black, values larger than 0.9, in dark gray, 0.5, in light gray 0.3, and 0.25

This case is also analyzed with the Okubo-Weiss [18], [21] criterion which does not take the rotation of deformation axes (i.e. $\dot{\phi}$) into account. Clearly, this criterion cannot locate the regions of strong deformation as accurately as the Lagrangian criterion [11]. In particular, according to the Okubo-Weiss criterion, deformation would be relatively isotropic around the vortices at $t = 0$ (figure 12). As seen on figure 9, this is not the case. Therefore, taking into account the rotation of deformation axes is essential: it strongly diminishes the effective deformation which is then localized in specific regions (compare figures 11 and 12). Furthermore, at $t = 1.11\tau$, the Okubo-Weiss criterion does not predict the strong deformation at the cusp of the separating filament.

²inner and outer must be understood here with reference to the center of the plane

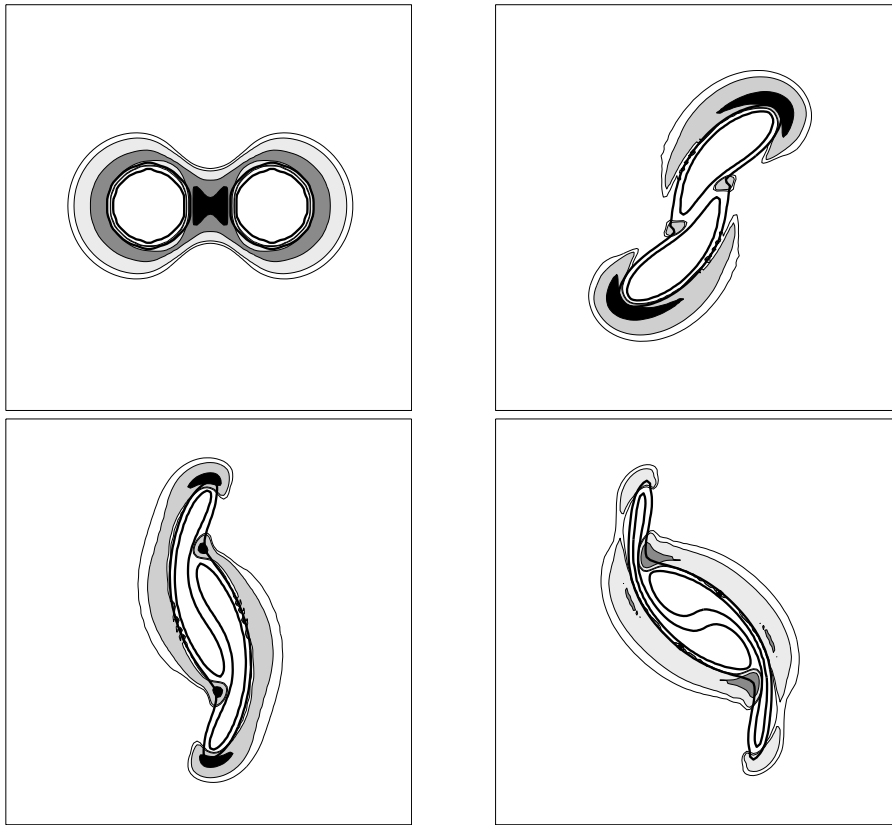


Fig. 12. Effective rate of deformation by Okubo-Weiss criterion at time $t = 0, 0.64\tau, 1.11\tau, 1.43\tau$ for the simulation of figure 9. In black, values larger than 0.9, in dark gray, 0.5, in light gray 0.3, and 0.25

Secondly, we examine the influence of various external strains on merger using the Lagrangian criterion derived by [11]. Table 7 shows, for several values of γ , the critical merger distance, the merger efficiency for the same initial distance ($d/r_0 = 2.83$) at time $t = 2.5\tau$, and the average deformation σ^{eff} in the vortex core and outside the vortices (average is taken in space and time before filamentation, i.e. for $t < 1.75\tau$).

As explained previously, the critical merger distance increases from negative to positive external strains (γ). But a larger merger efficiency for positive strain may seem paradoxical: indeed positive γ corresponds to larger total deformation and thus stronger filamentation could be expected. In fact, the paradox can be resolved by separating the role of deformation inside and outside the vortices. The deformation exerted around the vortices tends to deform the vortex boundary which will elongate and promote merger while the deformation exerted inside the vortices tends to split the vortices and favor filamentation. Table 7 shows that the deformation exerted on the vortex boundaries is larger for positive γ than for negative γ ; vortex elongation and collapse vary accordingly. This variation is consistent with the observed dependence of the critical merger distance on γ . On the other hand, the deformation exerted on the vortex cores is larger for negative γ leading to more filamentation; this is also consistent with the observed efficiency.

5.4. Merger efficiency

We now determine merger efficiency when the initial distance between vortices is not held constant. Different processes can affect efficiency, such as external strain, initial distance between the vortices and small scale dissipation. For equal initial distance, a positive external strain increases the efficiency while

a negative one decreases it. Increasing the distance between vortices will decrease the deformation exerted on them but, at the same time, will delay merger. The vortices will experience a smaller deformation but on a longer period, and the result on the filamentation is not straightforward to predict [12]. Also the small scale dissipation will constantly erode the vortices and decrease the efficiency of vortex merger.

Table 8 shows the merger efficiency taking into account all these effects. It is computed for an initial vortex distance equal to 90% of the critical merger distance and after a very long time compared to merger. Since filaments are created during merger to accommodate angular momentum conservation and are finally wiped out by viscosity, merger will never be a 100% efficient process. Merger efficiency is clearly maximum for zero external strain. We see that when varying accordingly the initial distance, the efficiency is almost independent of the sign of the external strain. Thus increasing the initial distance between vortices has an effect opposite to that of the sole external strain. Our interpretation is that a deformation applied longer elongates the vortices more efficiently.

6. Conclusions and openings

The influence of a large scale deformation field on the evolution of a vortex doublet in a two-dimensional incompressible fluid has been studied with analytical and numerical models. Equal and positive vorticity was chosen for the vortices (negative vorticity leads to symmetrical results with a change in sign of strain and global rotation).

Point vortex theory has evidenced that two identical vortices possess an equilibrium position in an external strain (if this strain amplitude is larger than external rotation). The nature of vortex trajectories depend on the initial location of the vortices (inside or outside of the fixed point). Point vortices initially close to each other rotate along an elliptical trajectory which was also observed for finite-area vortices, while initially distant vortices undergo strain-induced expulsion along open streamlines. This equilibrium position, unstable to orthoradial perturbation, was also observed numerically in the interaction of two finite-area vortices; its analytical characteristics were retrieved and confirmed by numerical simulations with a spectral model.

In an external strain, interacting vortices exhibit a dominant elliptical deformation of their contours, both in steady state calculations and in the spectral model. The elliptical model was therefore used to compute the doublet dynamics. The steady state, elliptical and spectral models confirmed that each vortex ellipticity is stronger with positive strain than in its absence. Moreover, the point vortex, elliptical and spectral models gave very consistent results concerning the ellipticity of the doublet trajectory for initially close vortices.

The spectral code evidenced four different nonlinear evolutions for the vortex doublet in the presence of strain: co-rotation, merger, stationarity and strain induced expulsion. Only the former two are found in the absence of external strain. Co-rotation of vortices along elliptical trajectories was already described hereabove. Stationary vortices are mostly deformed elliptically. Strain-induced expulsion of finite-area vortices obeys the rule obtained by point vortex theory (variation of critical distance with external strain and rotation). For merger, the critical distance increases with positive strain (and decreases with negative strain). As expected, external rotation favors co-rotation of the doublet against its merger.

These variations of the critical merger distance and of merger efficiency with external parameters, have lead to a closer inspection of vortex deformation and of the filamentation process using a Lagrangian criterion in the spectral code. Indeed, the elliptical deformation is not the only one induced on each vortex by strain and by its companion. The Lagrangian analysis indicates that each vortex is submitted to an asymmetric deformation, stronger on the side facing the other vortex than on the opposite side. This asymmetry elongates the inner side of each vortex more than their outer side and promotes merger. Moreover, the influence of the external flow on the vortex doublet depends on the

sign of γ : for a given initial distance, positive γ promotes merger with a larger efficiency than for negative γ , by increasing the deformation of the outer vortex boundary. On the contrary, when the initial distance between vortices is not held constant, the influence of the mutual strain also intervenes and merger efficiency decreases for both signs of external strain. Finally, it is observed that merger efficiency also depends on the duration of the merging process.

Merger is therefore not an all powerful mechanism for vortex growth as soon as external factors are involved. Large scale strain or shear has an essential influence on merger and filamentation efficiency. For an application to two-dimensional turbulence, the present study provides useful information on the ability of small vortices (formed by the wrap-up of filaments) to merge, in the strain or shear flow imposed by the large coherent vortices. This shear or strain rate can most often be computed numerically. Such calculations should be performed with numerical simulations of turbulence in the future, to validate our simple approach. For an application to oceanic vortex dynamics, the present study should be extended to stratified flows by using a finite deformation radius. Recently, two deep vortices were observed to interact (but not merge) southwest of Portugal. Application of our criteria to the data will help determine the relative influence of large scale strain (due to surrounding currents), of beta effect (variable Coriolis parameter) and of stratification on this interaction.

Acknowledgements

This work is a contribution to the SEMANE research program supported by IFREMER and by SHOM/CMO (French Navy Oceanographic Center). Thanks are due to Dr Bernard Legras (LMD Paris) and to Pr David Dritschel (Maths Dpt, Univ. St Andrews, Scotland) for fine suggestions and comments.

Tables

Table 1. Critical distance between vortex centers (below which merger should occur) versus γ in elliptical model

γ	0	0.044	0.089	0.133	0.178	0.356	0.534	0.712
d/r	3.25	3.30	3.43	3.53	3.63	4.05	3.85	3.45

Table 2. Aspect ratio of co-rotating vortex trajectories versus γ . *sp* stands for spectral code, *em* for elliptical model and *pv* for point vortex theory

γ	0	0.044	0.089	0.133	0.178
λ_{sp}	1	0.91	0.84	0.76	0.70
λ_{em}	1	0.88	0.79	0.70	0.63
λ_{pv}	1	0.90	0.80	0.70	0.60

Table 3. Aspect ratio of vortex versus γ . *sp* stands for spectral code and *em* for elliptical model

γ	0	0.044	0.089	0.133	0.178
λ_{sp}	0.82	0.81	0.80	0.80	0.79
λ_{em}	0.89	0.87	0.84	0.83	0.81

Table 4. Critical merger distance in the spectral code for negative strain

γ	-0.178	-0.133	-0.089	-0.044	0
d/r_{sp}	3.15	3.15	3.20	3.30	3.35

Table 5. Comparison of critical merger distance between spectral code sp and the elliptical model em

γ	0	0.044	0.089	0.133	0.178
d/r_{sp}	3.35	3.4	3.5	3.6	3.7
d/r_{em}	3.25	3.3	3.43	3.53	3.63

 Table 6. Critical merger distance for $\omega = \pm\gamma$. sp stands for spectral code and em for elliptical model

$\gamma = \omega$	0.044	0.089	0.133	0.178
d/r_{sp}	3.45	3.6	3.7	3.9
d/r_{em}	3.32	3.48	3.58	3.68
$\gamma = -\omega$	0.044	0.089	0.133	0.178
d/r_{sp}	3.35	3.4	3.45	3.5
d/r_{em}	3.25	3.35	3.45	3.55

 Table 7. Filamentation analysis for $d/r_0 = 2.83$

γ	-0.178	-0.133	0.133	0.178
d/r	3.15	3.15	3.65	3.70
$\kappa_{final}/\kappa_{initial}$	0.798	0.800	0.847	0.855
$\sigma_{outside}^{eff}$	0.0182	0.0179	0.0193	0.0200
σ_{inside}^{eff}	0.0763	0.0763	0.0746	0.0743

 Table 8. Merger efficiency for $d/r_0 = 0.9 d_{critical}/r_0$

γ	-0.178	-0.133	-0.089	-0.044	0
$\kappa_{final}/\kappa_{initial}$	0.797	0.820	0.835	0.846	0.855
γ	0	0.044	0.089	0.133	0.178
$\kappa_{final}/\kappa_{initial}$	0.855	0.851	0.846	0.820	0.798

References

- [1] *C. Bertrand, X. Carton.* Vortex merger on the β -plane. *C. R. Acad. Sci. Paris.* 1993. T. 316, II. P. 1201–1206.
- [2] *P. Capéran, J. Verron.* Numerical simulation of a physical experiment on two-dimensional vortex merging. *Fluid Dyn. Res.* 1988. V. 3. P. 87–92.
- [3] *G. F. Carnevale, P. Cavazza, P. Orlandi, R. Purini.* An explanation for anomalous vortex merger in rotating-tank experiments. *Phys. Fluids.* 1991. V. A3. P. 1411–1415.
- [4] *X. Carton.* On the merger of shielded vortices. *Europhys. Lett.* 1992. V. 18. P. 697–703.
- [5] *X. Carton.* Hydrodynamical modeling of oceanic vortices. *Surveys in Geophys.* 2001. V. 22. P. 179–263.
- [6] *X. Carton, B. Legras, G. Maze.* Two-dimensional vor-

- tex merger in an external strain field. *Journal of Turbulence*. 2002. V. 3. Article 045 (IoP electronic publication).
- [7] [B. Cushman-Roisin, B. Tang](#). Geostrophic turbulence and the emergence of eddies beyond the radius of deformation. *J. Phys. Oceanogr.* 1990. V. 20. P. 97–113.
- [8] *D. G. Dritschel*. The stability and energetics of corotating uniform vortices. *J. Fluid Mech.* 1985. V. 157. P. 95–134.
- [9] *D. G. Dritschel*. The stability of elliptical vortices in an external straining flow. *J. Fluid Mech.* 1990. V. 210. P. 223–261.
- [10] *D. G. Dritschel, D. Waugh*. Quantification of the inelastic interaction of unequal vortices in two-dimensional vortex dynamics. *Phys. Fluids*. 1992. V. A4. P. 1737–1744.
- [11] [G. Lapeyre, P. Klein, B. L. Hua](#). Does the tracer gradient vector align with the strain eigenvectors in 2D turbulence? *Phys. Fluids*. 1999. V. 11. P. 3729–3737.
- [12] [G. Lapeyre, B. L. Hua, B. Legras](#). Comment on "Finding finite-time invariant manifold in two-dimensional velocity fields". *Chaos*. 2001. V. 11. P. 427–430.
- [13] *B. Legras, D. G. Dritschel*. The elliptical model of two-dimensional vortex dynamics. *Phys. Fluids*. 1991. V. A3. P. 845–869.
- [14] [M. V. Melander, N. J. Zabusky, J. C. McWilliams](#). Asymmetric vortex merger in two dimensions: which vortex is "victorious"? *Phys. Fluids*. 1987. V. 30. P. 2604–2610.
- [15] *M. V. Melander, N. J. Zabusky, J. C. McWilliams*. Symmetric vortex merger in two dimensions. *J. Fluid Mech.* 1988. V. 195. P. 303–340.
- [16] *J. C. McWilliams*. The emergence of isolated coherent vortices in turbulent flow. *J. Fluid Mech.* 1984. V. 146. P. 21–43.
- [17] *J. C. McWilliams*. The vortices of two-dimensional turbulence. *J. Fluid Mech.* 1990. V. 219. P. 361–385.
- [18] *A. Okubo*. Horizontal dispersion of floatable particles in the vicinity of velocity singularities such as convergences. *Deep-Sea Res.* 1970. V. 17. P. 445–454.
- [19] [K. Schultz-Tokos, H. H. Hinrichsen, W. Zenk](#). Merging and migration of two meddies. *J. Phys. Oceanogr.* 1994. V. 24. P. 2129–2141.
- [20] *D. Waugh*. The efficiency of symmetric vortex merger. *Phys. Fluids*. 1992. V. A4. P. 1745–1758.
- [21] *J. Weiss*. The dynamics of enstrophy transfer in two-dimensional hydrodynamics. LJI-Tn-81-121 report. La Jolla Institute, La Jolla, CA. 1981.
- [22] [H. M. Wu, E. A. Overman II, N. J. Zabusky](#). Steady states of the Euler equations in two dimensions. Rotating and translating V-States with limiting cases. I. Numerical algorithms and results. *J. Comp. Phys.* 1984. V. 53. P. 42–71.
- [23] [I. Yasuda, G. R. Flierl](#). Two-dimensional asymmetric vortex merger: merger dynamics and critical merger distance. *Dyn. Atmos. Oceans*. 1997. V. 26. P. 159–181.